

Anticlinic order of long-range repulsive rod-like magnetic particles in 2D

Xiaoyu Zheng^{1,*}, Obeng Appiagyei Addai^{1,†}, Peter Palffy-Muhoray^{1,2,‡}

¹*Department of Mathematical Sciences, Kent State University, OH, USA*

²*Advanced Materials and Liquid Crystal Institute, Kent State University, OH, USA*

February 2, 2022

Abstract

In the field of liquid crystals, it is well-known that rod-like molecules interacting via long-range attractive interactions or short-range repulsive potentials can exhibit orientational order. In this work, we are interested in what would happen to systems of rod-like particles interacting via long-range repulsive potential. In our model, each particle consists of a number of point dipoles uniformly distributed along the particle length, with all dipoles pointing along the z -axis, so that the rod-like particles repel each other when they lie in the $x-y$ plane. Dipoles from different particles interact via an r^{-3} potential, where r is the distance between the dipoles. We have considered two model systems, each with N particles in a unit cell with periodic boundary conditions. In the first, particle centers are fixed on a square or triangular lattice but they are free to rotate. In the second, particles are free to translate as well as in cells with variable shapes. Here they self-assemble to form configurations where the stress tensors are isotropic. Our numerical results show that at low temperatures the particles tend to form stripes with alternating orientations, resembling herringbone patterns or the anticlinic Sm- C_A liquid crystal phase.

1 Introduction

It is well known that systems of rod-like molecules form the nematic phase under certain circumstances. For thermotropic liquid crystals, the rod-like molecules interact via induced dipole-dipole interactions. This long-range attractive forces between molecules promotes alignment with each other. At sufficiently low temperatures, the Helmholtz free energy of the system is minimized when the molecules more or less align with each other, resulting in long-range orientational order [1]. On the other hand, hard rod systems, in which particles interact via a short-range hard-core interparticle potential, form the nematic phase for certain aspect ratios above certain packing fractions. The free energy depends solely on the entropy, which is a measure of the orientation dependent free volume of the system. At sufficiently high packing fractions, the rod-like particles form orientational order, giving up the orientational entropy in order to gain translational entropy [2].

It is interesting to ask whether a system of anisometric particles interacting with a long-range repulsive potential will spontaneously form orientational order. To answer this question is the motivation for this work.

An immediate example of repulsive particles are discrete point charges with the same sign interacting via pairwise r^{-1} potential, where r is the distance between charges. Wigner predicted that a gas of electrons at zero temperature form a bcc lattice in 3D [3]. Two-dimensional experiments showed that at low temperatures and high areal density, a sheet of electrons crystalized into a triangular lattice in 2D [4], which is known as a Wigner crystal. Montgomery [5] proved that for particles in a 2D Bravais lattice interacting with pairwise r^{-s} potential with fixed density, the triangular lattice is the unique minimizer for any real $s > 0$.

*Corresponding author, Email: xzheng3@kent.edu, ORCID 0000-0002-3787-7741

†Email: oaddai@kent.edu, ORCID 0000-0003-0024-7989

‡Email: mpalffy@kent.edu, ORCID 0000-0002-9685-5489

An example of a system of particles interacting via an r^{-3} potential is a system of discrete point electric or magnetic dipoles. In one realization, the centers of the dipoles are confined to a 2D planar region, and the direction of the dipoles are constrained to be along the normal to the plane and all point in the same direction, so that they repel each other. Experiments on 2D colloidal superparamagnetic particles interacting via repulsive magnetic dipolar interactions clearly showed that the systems form a crystal phase with a triangular lattice at low temperatures [6, 7], consistent with the results in [5].

Here, we consider particles consisting of two or more dipoles in the z -direction, fixed on a long rod which lies in the $x - y$ plane. The rods repel each other. A realistic object resembling this model is a thin slab of magnetic material, magnetized through its thickness, lying in the plane. *A collection of such slabs serves as a primitive model of the system that we want to study in this work.* The pair potential may be separated into an isotropic and an anisotropic part. The isotropic part accounts for the interactions without regard to the shape, and the anisotropic part for the interactions due to the shape or the anisotropic distribution of dipoles. As discussed below, at low number densities, the isotropic interactions dominate, so one expects that the particle centers form a crystal structure similar to that of point charges or dipoles. As the number density increases, the anisotropic repulsive interactions become predominant, so that the particle positions and orientations become correlated. Therefore at high densities, the low density crystal structure may be destroyed or deformed and new ordered structures may appear. We are interested in finding these new ordered structures and in understanding their density dependence.

A system of rod-like particles with long-range repulsion has been studied in 3D [8]. The authors confined charged rod-like colloids in a thin wedged-shaped cell and showed that the position and orientational order of the colloids depends on the interaction with the cell walls. In our work, we study configurations either formed by the particles alone, without external constraints, or where the orientations of the particles are not affected by external constraints.

The paper is organized as follows. Section 2 lays out the mathematical model describing the interactions between the particles in our system. Section 3 discusses the model systems that we are interested in and the numerical procedures which lead to the identification of equilibrium states. Section 4 presents the numerical results on systems of particles on square and triangular lattices and on particles in cells with variable shapes and we conclude in Section 5.

2 Mathematical Model

In this work, we ignore thermal effects and the kinetic energy of particles. We look for configurations which correspond to minima of the potential energy. The total potential energy of the system of N particles, assuming pairwise interactions, is given by

$$E = \frac{1}{2} \sum_{i=1}^N \sum_{j \neq i}^N w(\mathbf{q}_i, \mathbf{q}_j), \quad (1)$$

where $\mathbf{q}_i = (\mathbf{r}_i, \theta_i)$ is the generalized coordinate of particle i , with $\mathbf{r}_i = (x_i, y_i)$ the coordinates of the center, and θ_i the angle formed by the long axis of the particle with the x -axis. The system may be subject to external constraints, for example, geometric confinements or periodic boundary conditions.

We model each particle as a long rod with n uniformly distributed point dipoles along the particle length, where all the dipoles point along the z -direction. We set the width of each particle to be zero, as the width does not play a role in our model, so the particle shape is a line segment. The interpenetration of the particles or of the line segments, is prohibited. One can also consider particles as being made up by two lines of charges of finite length, with the line of positive charges above the plane, and the line of negative charges beneath the plane. Our model of particles with discrete dipoles is an approximation of a line of dipoles with finite length, with dipoles pointing to the z -direction. With this in mind, the interaction between two particles can be modeled by the sum of all pair interactions between dipoles, excluding dipole pairs on the same particle,

$$w(\mathbf{q}_i, \mathbf{q}_j) = \sum_{k=1}^n \sum_{l=1}^n w_{(i,k)(j,l)}. \quad (2)$$

Here we use the notation $w_{(i,k)(j,l)}$ to denote the interaction energy of the k^{th} dipole on i^{th} particle and l^{th} dipole on j^{th} particle. The interaction energy of two permanent magnetic point dipoles is given by [12]

$$w_{ab} = -\frac{\mu_0 m_a m_b}{4\pi r^3} (3(\hat{\mathbf{m}}_a \cdot \hat{\mathbf{r}})(\hat{\mathbf{m}}_b \cdot \hat{\mathbf{r}}) - (\hat{\mathbf{m}}_a \cdot \hat{\mathbf{m}}_b)) = \frac{\mu_0 m_a m_b}{4\pi r^3}, \quad (3)$$

where μ_0 is the permeability of free space, $\mathbf{m}_a = m_a \hat{\mathbf{z}}$ is the dipole moment and $\mathbf{r} = r \hat{\mathbf{r}}$ is the vector from \mathbf{m}_b to \mathbf{m}_a .

In the minimum energy configuration, the force and torque on each particle are zero. The total force on each particle is the sum of forces on all dipoles on the particle,

$$\mathbf{F}_i = \sum_{k=1}^n \mathbf{F}_{i,k}, \quad (4)$$

where $\mathbf{F}_{i,k}$ is the force acting on the k^{th} dipole of particle i , with

$$\mathbf{F}_{i,k} = \sum_{j \neq i}^N \sum_{l=1}^n \mathbf{F}_{(i,k)(j,l)}, \quad (5)$$

and $\mathbf{F}_{(i,k)(j,l)}$ is the force acting on the k^{th} dipole of particle i due to the l^{th} dipole of particle j . One can readily calculate the force \mathbf{F}_{ab} on \mathbf{m}_a due to the presence of \mathbf{m}_b as the negative gradient of the pair potential,

$$\mathbf{F}_{ab} = -\nabla w_{ab} = \frac{3\mu_0 m_a m_b}{4\pi r^4} \hat{\mathbf{r}}. \quad (6)$$

The torque on each particle with respect to the particle center is the sum of torques on all the dipoles on the particle,

$$\boldsymbol{\tau}_i = \sum_{k=1}^n (\mathbf{r}_{i,k} - \mathbf{r}_i) \times \mathbf{F}_{i,k}. \quad (7)$$

We define the number density $\rho = N/A$, where A is the area of the region containing the particles. There are three lengths in our system: domain size, particle size, and mean interparticle distance $\sqrt{1/\rho}$. We define the particle length l as the distance between the two farthest dipoles on a particle. If we scale all the lengths by the particle length l , and scale the dipole moments by m_0 , then the scaled pair potential and force between two dipoles are

$$\bar{w}_{ab} = \frac{w}{\mu_0 m_0^2 / 4\pi l^3} = \frac{1}{r_c^3}, \quad (8)$$

$$\bar{\mathbf{F}}_{ab} = \frac{\mathbf{F}_{ab}}{\mu_0 m_0^2 / 4\pi l^4} = \frac{3}{r_c^4} \hat{\mathbf{r}}, \quad (9)$$

where r_c is the normalized distance between two point dipoles.

We consider the elementary case of two particles centered along the x -axis and separated by a distance d . The pair interaction energy, if $d \gg 1$, can be written as

$$\bar{w}(d, \theta_1, \theta_2) = \frac{n^2}{d^3} + \frac{(n+1)n^2}{16(n-1)d^5} [6 + 5(\cos 2\theta_1 + \cos 2\theta_2)] + O\left(\frac{1}{d^7}\right), \quad (10)$$

where the first term is an isotropic term in which only centers matter, and the rest contain orientation dependent anisotropic terms. Considering only the first two terms, the minimum occurs when $\theta_1 = \theta_2 = \pi/2$. Keeping more terms makes it difficult to determine where the minimizer is analytically. Instead, we plot the energy contours in terms of the orientations of the two particles. A typical plot is shown in Fig. 1(a) with the number of dipoles $n = 21$ at a distance $d = 1.6$. The energy contour plots show that the minimum energy state occurs when $\theta_1 = \theta_2 = \pi/2$, for any $d > 0$. That is, they are parallel to each other and both are perpendicular to the line connecting the centers, as shown in Fig. 1(b1). The energy attains its maximum when they are both parallel to the line connecting the centers, as shown in Fig. 1(b2), and attains its saddle

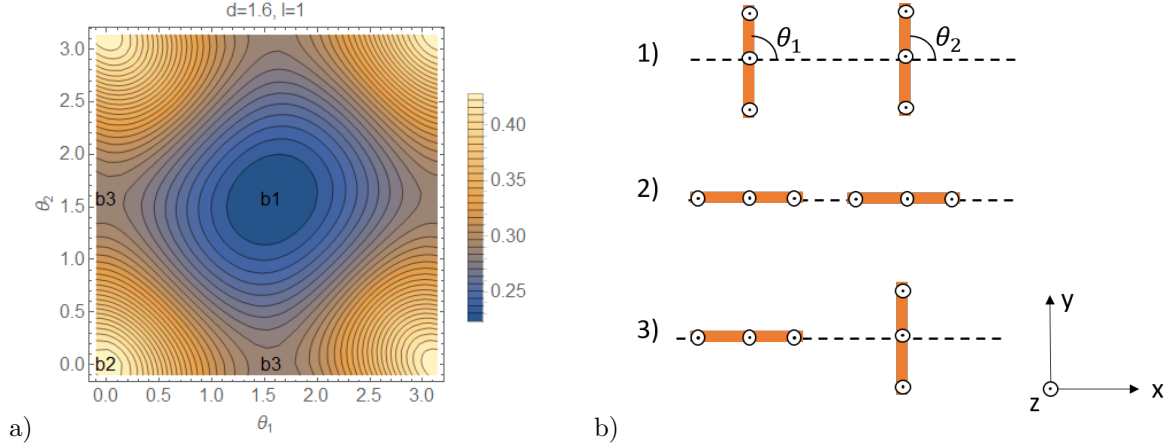


Figure 1: (a) Representative energy contours of two particles separated on the x -axis by a distance of $d = 1.6$ as function of the angles θ_1 and θ_2 . The number of dipoles on each particle is $n = 21$. The minimum energy state is attained when both angles are $\pi/2$, corresponding to the configuration in (b1). The maximum energy state is attained when both angles are zero, corresponding to the configuration in (b2). If $\theta_1 = 0$, then the minimum energy state is attained when $\theta_2 = \pi/2$, corresponding to the configuration in (b3). In the schematic of (b), only three dipoles are shown on each particle to illustrate the directions of dipoles.

point when one aligns along the x -direction and the other along the y -direction, as in Fig. 1(b3). If the separation distance between the centers is too short, then the configurations in (b2) and/or (b3) in Fig. 1 cannot be attained as the particles will interpenetrate, but the minimum energy state is still attained at the configuration in (b1), which is the minimizer of the anisotropic part of the energy.

If we consider the one-dimensional problem where a number of such particles, whose centers are constrained to be on an interval on the x -axis, with periodic boundary conditions, then in the minimum energy state the centers of the particles are uniformly distributed in the interval and all particles are parallel to the y -axis. In two dimensions, this simple configuration where all particles are aligned parallel to the y -axis is no longer the minimum energy state. What configuration will minimize the total energy in this case? We try to answer this question in two model systems detailed below.

3 Model systems and numerical procedures

We are interested in systems where the particles will form patterns in a 2D plane. For this, we have considered two specific model systems: (a) systems where the particle centers are fixed on a given lattice, and (b) systems in which particles self-assemble into some recognizable configurations. In both cases, we consider a finite system with periodic boundary conditions.

In the first model system, there is an underlying lattice \mathbf{L} , where the particle centers are fixed at each lattice site, and the goal is to find particle orientations which minimize the total potential energy. The underlying lattice can be regarded as an external constraint, but such a constraint will not directly influence the orientations of particles. In this case, the energy of the system is given by

$$E_L = \frac{1}{2} \sum_{i \neq j \in \mathbf{L}} w(\mathbf{q}_i, \mathbf{q}_j). \quad (11)$$

Here the sum is over all lattice sites. Since analytic expressions for the sum are unavailable, we solve the problem numerically. Our numerical procedure is as described below.

We first partition an infinite lattice into identical unit cells, in the shape of parallelograms, each containing a number of lattice sites. The unit cell is then surrounded by 8 congruent image cells. If we denote the edges of a unit cell by vectors \mathbf{a} and \mathbf{b} , and denote the matrix $H = [\mathbf{a}, \mathbf{b}]$, then the area of the cell is given by $A = \det H$. The position of the center of particle i can be expressed as a linear combination of the

two basis vectors as $\mathbf{r}_i = \xi_i \mathbf{a} + \eta_i \mathbf{b} = H \mathbf{t}_i$, where $\mathbf{t}_i = (\xi_i, \eta_i)'$ is the relative coordinate of the particle i with $0 < \xi_i, \eta_i < 1$. The centers of particles in the image cells can be assigned as $\mathbf{r}_i + H \mathbf{n}$, where $\mathbf{n} = (n_1, n_2)'$, with integer components ranging from -1 to 1 . Our numerical simulation starts with a given initial orientations of all particles on the lattice sites in the unit cell, which is then copied to all image cells. We next calculate the torque on each particle according to Eq. (7). We assume that the contributions to the torque on a particle from dipoles far away have a minimal effect comparing to that from the nearby dipoles, thus the torque on each particle is only calculated from dipoles within a cutoff radius. Specifically, for each dipole on a particle, all dipoles on other particles within a radius r_0 , including those in the image cells, will be included in the torque calculation, and dipoles outside will have no contribution. In this work, the radius r_0 is taken to be the length of the short side of the unit cell. We approach the equilibrium using overdamped dynamics; we advance the system by a timestep Δt where each particle rotates with angular velocity proportional to the torque acting on it. Discretizing this, the angles are updated as

$$\theta_i(t + \Delta t) = \theta_i(t) + \beta \tau_i \Delta t, \quad i = 1, \dots, N, \quad (12)$$

where β is proportional to the reciprocal of rotational viscosity and N is the number of lattice sites, or equivalently the number of particles in the unit cell. Once the orientations of all particles in the unit cell have been updated and copied to all image cells, the new torque is evaluated for each particle based on the updated configuration. This process is repeated until the torques on all particles vanish or are within a tolerance of 10^{-12} .

In the second model system, we consider N particles free to move in a unit cell shaped as a parallelogram. Periodic boundary conditions are imposed as before such that the unit cell is surrounded by 8 congruent image cells. The simulation starts with given initial positions and orientations of the N particles in the unit cell, which is then copied to all image cells. Next, the force and torque exerted on each particle in the unit cell from neighboring dipoles within a cutoff radius are calculated according to Eqs. (4)–(7). Using discretized overdamped dynamics as before, each particle will then translate and rotate with velocity and angular velocity proportional to the force and torque,

$$\mathbf{r}_i(t + \Delta t) = \mathbf{r}_i(t) + \alpha \mathbf{F}_i \Delta t, \quad (13)$$

$$\theta_i(t + \Delta t) = \theta_i(t) + \beta \tau_i \Delta t, \quad (14)$$

where α and β are proportional to the reciprocals of the viscosity and angular viscosity, respectively. At each step, the orientations and positions of the particles are copied to all image cells. This process is repeated until the forces and torques on all particles in the cell vanish. Our journey does not end here. Since the particles are not fixed on lattice sites, forces acting on them can give rise to stresses on the unit cell walls, which can change the shape of the unit cell at fixed number density.

For a given configuration, the average stress tensor acting on the unit cell can be calculated by [14]

$$\boldsymbol{\sigma} = \frac{1}{2A} \sum_{i,k} \sum_{j(\neq i),l} \mathbf{F}_{(i,k)(j,l)} (\mathbf{r}_{(i,k)} - \mathbf{r}_{(j,l)}), \quad (15)$$

where the outer sum indices are over the dipoles in the central unit cell, and the inner sum indices are over the dipoles in central unit cell as well as the image cells, excluding the dipole pairs on the same particle. We assume that the unit cell deforms in response to stress similarly to a volume conserving elastic body. If the stress tensor is not isotropic, the shape of the unit cell will change [13]. In our simulation, since the stress is symmetric, we have kept the vector $\mathbf{a} = (a, 0)$ parallel to the x -axis, and let $\mathbf{b} = (b_x, b_y)$ free to rotate. Specifically, the length of \mathbf{a} is updated by

$$a'_x = a_x + W b_y (\sigma_{xx} - \sigma_{yy}), \quad (16)$$

where W is proportional to the reciprocal of elastic modulus, and

$$b'_y = \frac{A}{a'_x}, \quad (17)$$

such that the area of the parallelogram remains as a constant. The x -component of vector \mathbf{b} is updated as

$$b'_x = b_x + W a_x \sigma_{xy}. \quad (18)$$

Our simulation is in clear contrast from the traditional constant pressure simulation, where a pressure tensor is imposed; rather, it is a constant volume (area, in our case), variable cell shape simulation. The equilibrium configurations correspond to the cell shapes which admit isotropic stress tensors.

The final goal is to find the specific shape of the parallelogram such that the stress tensor is isotropic, at which point the total energy is minimized over all possible parallelograms with constant area.

We remark that when we consider the dipole interactions within a cutoff radius, it is not always meaningful to compare the energies of the systems with different underlying lattices, or even for particles on the same lattice but with different particle orientations. There are two main reasons for this. First, the energy decays slowly as function of system size. Second, the number of participating dipoles is not always the same for different configurations, and the energy calculation is largely dependent on the number of pairs of dipoles involved. We therefore rely on the calculations of torques and forces which vanish in equilibrium.

In general, there are multiple local energy minima, representing the rugged energy landscape. We have carefully selected the simulation parameters so that we can find the global minimum energy states and avoid frustrations by only locally favored configurations.

4 Results

In this section, we present numerical findings of the two model systems mentioned in Sect. 3. In the first model system, particle centers are fixed at the sites of two simple lattices: a square lattice and triangular (or hexagonal) lattice, and the particles are free to rotate about their centers. In the second model system, particles are free to translate as well as rotate in a cell with variable shape and constant area.

4.1 Particles on square lattices

We first consider the case when the centers of particles are fixed on sites of a square lattice. In this numerical experiment, the lattice size is varied to account for different number densities ρ . We have considered the cases where the total number of particles $N = 16, 36, 64, 100$ on a square lattice in a unit cell. The results of the angles θ_i for different values of N agree to within 10^{-4} for all number densities. Therefore, here we only present the representative results for $N = 36$ with $n = 9, 21$ and 41 dipoles on each particle.

Figure 2(a) shows some representative equilibrium configurations of particles on square lattices at several number densities, with $n = 41$ dipoles on each particle. For small values of ρ , that is, when the particles are far apart, they align uniformly along one diagonal of the lattice. In this configuration, the forces and torques from the four nearest neighbor particles as well as from the four neighbors at the nearest diagonal sites cancel exactly. As ρ increases above a critical number density, the configuration with the uniform alignment is no longer stable, as dipoles at the two nearest diagonal sites along the orientation of particles are so close that along the diagonal neighbor interactions dominate, and the configuration becomes unstable. To lower the energy, the particles on the neighboring sites rotate in opposite directions by the same amount, which results in the configurations that all particles along any diagonal, which is parallel to southwest-northeast direction, form a stripe. Furthermore, in each stripe the particles are aligned in the same direction, and the orientations alternate from stripe to stripe. The average orientation of all particles is parallel to the direction of the stripe. This configuration is also known as herringbone pattern.

Figure 2(b) shows the angles of particles in two adjacent stripes as a function of ρ . Different curves correspond to the results from $n = 9, 21, 41$, respectively. The critical number densities where there is a configurational transition from uniform alignment to the herringbone pattern occurs at $\rho_c \approx 0.8175, 0.9139, 0.9536$ for $n = 9, 21, 41$, respectively. Larger values of n shift the transition towards $\rho_c = 1$. At high densities, the particles are getting close and their neighbors can no longer be regarded as a continuous uniform body for small values of n . As a result, the angle θ as function of ρ for $n = 9$ does not follow a smooth curve, but instead oscillates about a smooth curve when $\rho \gtrsim 10$. The curves of θ in terms of ρ for $n = 21, 41$ also oscillate but the oscillating behavior is deferred to higher densities, where the numbers of dipoles per particle are not large enough to be regarded as continuously distributed. From the simplest geometric view, we anticipate that the orientation of particles becomes more and more parallel to the stripe direction as ρ increases for particles with continuously distributed dipoles along their lengths.

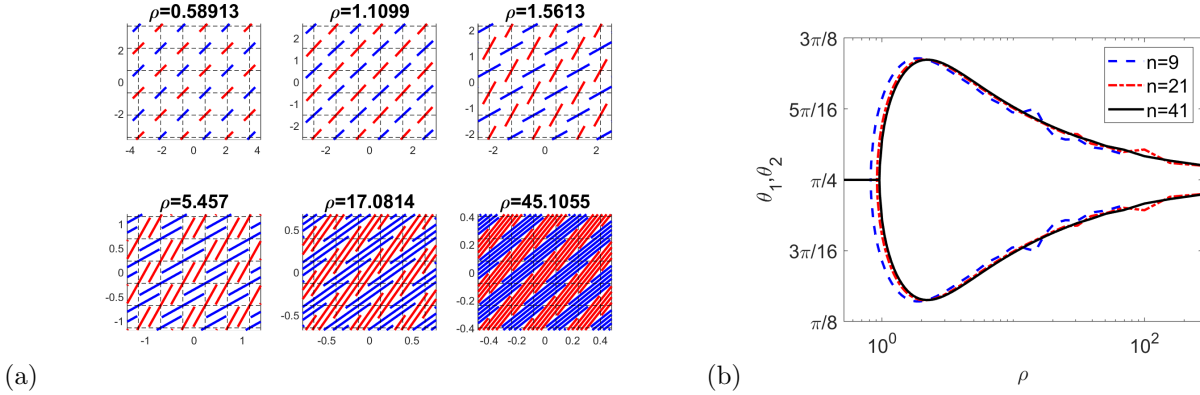


Figure 2: (a) Equilibrium configurations of particles on a square lattice at 6 representative number densities. Each particle has 41 uniformly distributed dipoles along its length. (b) The angles of particles in two adjacent stripes on the square lattices as a function of the number density ρ .

4.2 Particles on triangular lattices

Next, we fix the centers of particles on a triangular lattice. The numerical procedure and simulation parameters are exactly the same as those on the square lattices.

Figure 3(a) shows representative equilibrium configurations of particles on triangular lattices at several number densities. The orientations of the particles always form horizontal (or along any grid lines due to the three-fold symmetry) stripes on a triangular lattice, with alternating orientations from stripe to stripe. On average, all particles point along the stripe direction. Figure 3(b) shows the angles of the particles in two adjacent stripes as a function of ρ . Each curve corresponds to $n = 9, 21, 41$, respectively. Large numbers of dipoles per particle make the angle between the particles in adjacent stripes slightly larger. As $\rho \rightarrow 0$, the particle orientations saturate at $\theta_1 = -\theta_2 = \pi/4$. As ρ increases, the particles will tend to align with the stripe direction.

The results from the square and triangular lattices share one feature: the particles at high densities form stripes with alternating orientations.

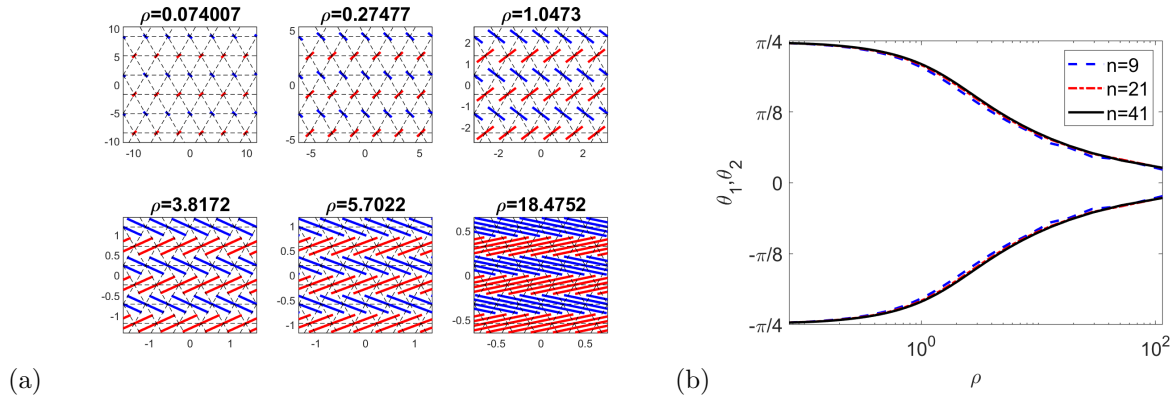


Figure 3: (a) Equilibrium configurations of particles on a triangular lattice at 6 representative number densities. Each particle has 41 uniformly distributed dipoles. (b) The angles of the particles in two adjacent stripes on the triangular lattices as a function of the number density ρ .

4.3 Free particles in a cell with variable shape

One can find the equilibrium configurations of particles with different underlying lattices and number densities following the same procedure. However, we are more interested in the question of whether particles would spontaneously organize themselves and form a lattice? If so, what lattices would be most likely to form at different number densities?

As we have indicated earlier, at a given number density, the unit cell containing the particles will adopt a shape such that the stress tensor of the corresponding equilibrium configuration is isotropic. In fact, the square and triangular lattices do not give rise to isotropic stress tensors. In the square lattice case, the normal stress components are the same, but the shear component is nonzero. In the triangular lattice case, the normal stress components differ.

We have carried out simulations of N particles in a unit cell under the periodic boundary conditions, with different initial conditions and numbers of particles. Since our goal is to identify the lattice formed by particles, we redefine the unit cell to be nearly square during the course of the simulation in order to maximize the cutoff length.

Preliminary results suggest that the particles tend to arrange themselves in a centered rectangular lattice. Furthermore, the particles at the rectangular vertices of the lattice have the same orientation, and the ones in the center of the lattice have opposite orientations such that the average angle is close to 0. With this in mind, we have rerun the simulations with centers of particles at a centered rectangular lattice, and assign an angle θ to particles on the rectangular vertices and assign the angle $-\theta$ to particles located at the center of the lattice. We then find the angle θ and the aspect ratio of the lattice as a function of ρ , where we define the aspect ratio of the centered rectangular lattice as the ratio of short side of the rectangle and the long side.

Our final results are summarized in Fig. 4. For small number densities, we have considered 10×10 particles in a unit cell. Several representative equilibrium configurations are shown in Fig. 4(a) with different number densities. The unit cell is bounded by thin solid lines, and the centered rectangular lattices are indicated by the dashed lines. We have used different numbers of dipoles $n = 9, 21$, and 41 on each particle as before. In Fig. 4(a) we show the results from $n = 41$. At high densities, since the aspect ratio of the lattice is very small, the unit cell is far from a square, so we considered more particles in the horizontal direction and less in the vertical direction, e.g., 30×4 or 18×2 , whose results are plotted in Fig. 4(b,c) at high number densities.

At low densities, the particles are far apart, so they can be regarded as point particles and the shape anisotropy does not play a significant role in determining the position of centers, and the lattice formed by the particle centers turns out to be very close to a triangular lattice. If we regard the triangular lattice as a special case of a centered rectangular lattice, then its aspect ratio corresponds to $1/\sqrt{3} \approx 0.577$. This is consistent with the result that repulsive point particles, interacting via the r^{-s} , $s > 0$ potential, form a triangular lattice in 2D [5]. As shown in Fig. 4(a), the particles form horizontal stripes, similar to that in triangular lattices. The angles of particles in each stripe is close to $\pm\pi/4$ in the dilute limit, which agrees with the results from Sect. 4.2. As ρ increases, the particles get closer. If we assume an isotropic shrinkage of the unit cell, it turns out that the vertical component of the stress tensor becomes larger than the horizontal component. In fact, if we only consider the contribution to the stress tensor from interactions of particles from the same stripe, not only does the horizontal component increase, but the vertical component also increases although by a smaller amount. If we consider the contribution to the stress tensor from particles from different stripes, the increase of the vertical component is much larger than that of the horizontal component. As a result, the stress on the upper and lower boundaries is larger than on the left and right boundaries, thus the unit cell grows taller and thinner, and the aspect ratio of the lattice decreases. Up to $\rho \approx 4$, the angles of particles on adjacent horizontal stripes are very close to $\pm\pi/4$. This result is not very sensitive to the values of n , and the aspect ratio of the centered rectangular lattice is slightly larger for larger values of n , as shown in Fig. 4(b,c).

As ρ increases a little further, the angle θ first dips down slightly and then increases. As ρ gets extremely high to about $\rho \approx 10$, the angle θ starts to decrease while the aspect ratio of the lattice remains almost constant. We attribute this nonlinear behavior of θ as function of ρ to the finite number of dipoles considered. As we increase n to 21 and 41, the nonlinear behavior of θ persists, but is deferred to higher number densities. This is similar to what we have observed in Sect. 4.1. We have run simulations and confirmed that at a given density, as we increase n , the angle θ approaches the proximity of $\pi/4$. A compelling analytic argument for

this magic angle has yet to be found.

There are also equilibrium configurations in which particle centers form a centered rectangular lattice and all particles orient uniformly along one edge of the rectangle. However, those configurations represent unstable equilibria.

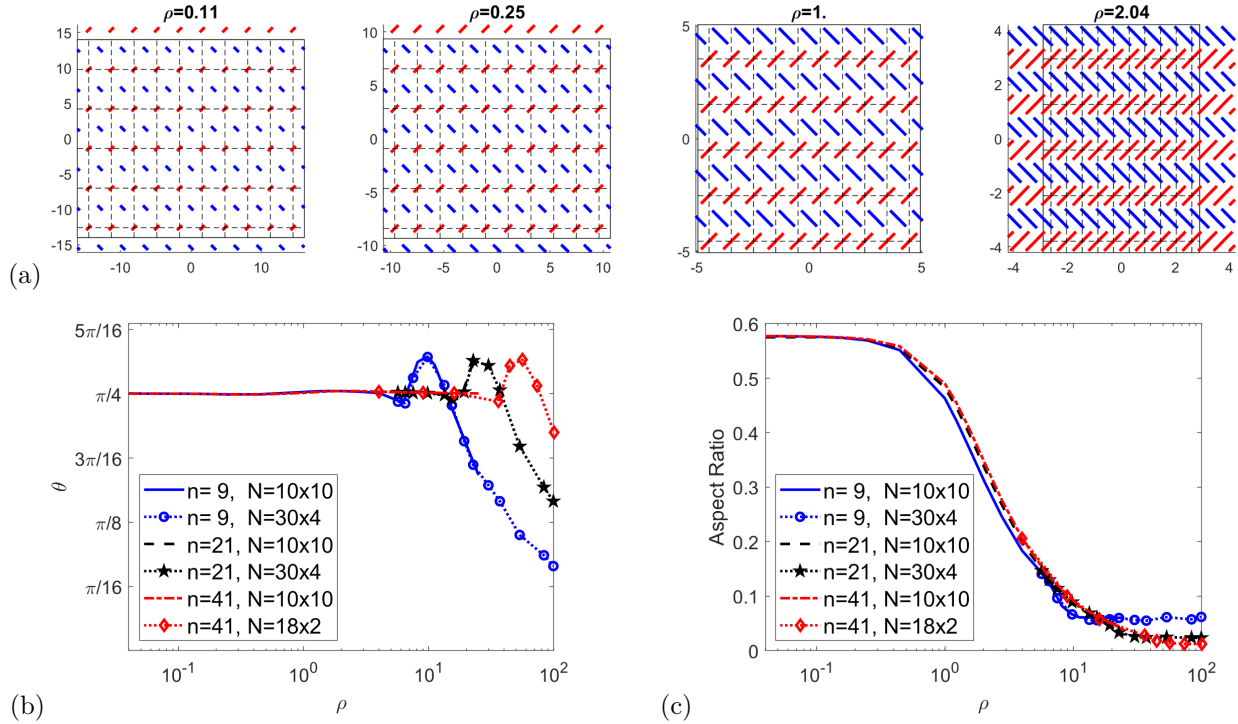


Figure 4: (Color online)(a) Equilibrium configurations of 100 free particles in a unit cell at 4 representative number densities. The unit cell is bounded by thin solid lines, and the centered rectangular lattice is indicated by the dashed lines. Each particle has 41 dipoles uniformly distributed along its length. The red particles are on the vertices of the centered rectangular lattice, and the blue particles are at the center of the lattice. (b) The angle of the particles on the vertices of the centered rectangular lattice as function of the number density ρ . (c) The aspect ratio of the centered rectangular lattice as function of the number density ρ .

5 Discussions and Conclusions

In this work, we have studied the equilibrium configurations of systems of rod-like particles interacting via long-range repulsive interactions in a two dimensional plane. We model those particles as line segments with uniformly distributed discrete point dipoles, with all dipoles pointing along the z -direction. We confine our study to dipoles interacting via an r^{-3} potential. We anticipate that the results will be qualitatively the same if the pairwise potential is r^{-s} with $s > 0$.

We have considered two model systems. In the first, we study the equilibrium orientations of particles with centers confined to a square or a triangular lattice. In the second, we study how particles self-assemble when they are free to translate and rotate in a cell with variable shape. In both model systems, periodic boundary conditions are imposed on a central unit cell containing N particles. We have chosen simulation parameters to prevent the formation of defects.

When the centers are fixed on a square lattice, particles will uniformly align along one of the diagonals in the dilute limit. As number density increases, there is a second order transition from the uniform alignment to the herringbone pattern where particles form stripes along the diagonals with alternating orientations from stripe to stripe. When the centers are fixed on a triangular lattice, the particles form the herringbone patterns for all number densities. When the particles are free to translate and rotate in a cell with variable

shape, the particles will self-assemble to form a centered rectangular lattice, where the angle of the particles on the rectangular vertices of the lattice is close to $\pi/4$ and the angle of the particle at the center of the lattice is close to $-\pi/4$. The lattice is close to a triangular lattice at dilute concentrations, and the aspect ratio of the lattice decreases as number density increases. Again, the particles form a herringbone structure with alternating orientations in adjacent stripes.

The herringbone structure is a key feature of the antiferroelectric smectic C_A phase formed by smectic liquid crystals consisting of elongated chiral molecules [15]. Systems of molecules with zigzag-shaped or bent core architectures can also exhibit the anticlinic phases [17]. In one of the molecular models [16], it has been shown that conventional dispersion and steric intermolecular interactions cannot stabilize the Sm- C_A phase, rather the orientational correlations between transverse molecular dipoles, when they are located in adjacent smectic layers, are responsible for stabilizing the Sm- C_A phase. In [18], the authors proposed that the presence of molecular-scale fluctuations of the layer interface between the smectic layers provide an entropic mechanism for exhibiting synclinic Sm-C order rather than the anticlinic Sm- C_A order. For materials exhibiting anticlinic order, the interface fluctuations might be suppressed due to their bent molecular conformation. To our knowledge, our system is the first system where solely long-range repulsive interactions are responsible for the formation of anticlinic order. Dipoles are as far as possible from each other in this anticlinic configuration.

If there is an external geometric constraint, for example, a finite number of particles are contained in a rectangular box, then the arrangement of particles will be very sensitive to the shape of the box and the number of particles. The equilibrium configuration will also depend on the interactions between the particles and the boundary walls.

In this study, thermal effects have been ignored. If thermal effects are included, at sufficiently high temperatures, the crystal structure formed by the centers of particles will melt, and orientational order will disappear. Other phases may possibly emerge. We defer this to a future study.

Conflicts of interest

There are no conflicts of interest to declare.

Acknowledgment

This work was inspired by a beautiful experiment made by Dr. Mykhailo Pevnyi when he was a graduate student at the liquid crystal institute at Kent state University. This work was supported by the Office of Naval Research through the MURI on Photomechanical Material Systems (ONR N00014-18-1-2624) and Air Force Research Laboratory through STTR grant: Electronically Dimmable Eye Protection Devices (FA8649-20-C-0011).

References

- [1] Maier, W. and Saupe, A. Z. Naturforsch. 13 a, 564-570 (1959); 14 a, 882-900 (1959); 15 a, 287-292 (1960).
- [2] Frenkel, D., 2015. Order through entropy. Nature materials, 14(1), pp.9-12.
- [3] Wigner, E., 1934. On the interaction of electrons in metals. Physical Review, 46(11), p.1002.
- [4] Grimes, C.C. and Adams, G., 1979. Evidence for a liquid-to-crystal phase transition in a classical, two-dimensional sheet of electrons. Physical Review Letters, 42(12), p.795.
- [5] Montgomery, H.L., 1988. Minimal theta functions. Glasgow Mathematical Journal, 30(1), pp.75-85.
- [6] Zahn, K., Lenke, R. and Maret, G., 1999. Two-stage melting of paramagnetic colloidal crystals in two dimensions. Physical review letters, 82(13), p.2721.

- [7] Gasser, U., Eisenmann, C., Maret, G. and Keim, P., 2010. Melting of crystals in two dimensions. *ChemPhysChem*, 11(5), pp.963-970.
- [8] Liu, B., Besseling, T.H., van Blaaderen, A. and Imhof, A., 2015. Confinement induced plastic crystal-to-crystal transitions in rodlike particles with long-ranged repulsion. *Physical review letters*, 115(7), p.078301.
- [9] Griffiths, D.J. and Li, Y., 1996. Charge density on a conducting needle. *American Journal of Physics*, 64(6), pp.706-714.
- [10] Andrews, M., 1997. Equilibrium charge density on a conducting needle. *American Journal of Physics*, 65(9), pp.846-850.
- [11] Jackson, J.D., 2002. Charge density on a thin straight wire: The first visit. *American Journal of Physics*, 70(4), pp.409-410.
- [12] Griffiths, D.J., 1962. *Introduction to electrodynamics*. New Jersey: Prentice Hall.
- [13] Parrinello, M. and Rahman, A., 1980. Crystal structure and pair potentials: A molecular-dynamics study. *Physical review letters*, 45(14), p.1196.
- [14] Louwse, M.J. and Baerends, E.J., 2006. Calculation of pressure in case of periodic boundary conditions. *Chemical physics letters*, 421(1-3), pp.138-141.
- [15] Takezoe, H., Gorecka, E. and Čepič, M., 2010. Antiferroelectric liquid crystals: interplay of simplicity and complexity. *Reviews of Modern Physics*, 82(1), p.897.
- [16] Osipov, M.A. and Fukuda, A., 2000. Molecular model for the anticlinic smectic-C A phase. *Physical Review E*, 62(3), p.3724.
- [17] Goodby, J.W., Mandle, R.J., Davis, E.J., Zhong, T. and Cowling, S.J., 2015. What makes a liquid crystal? The effect of free volume on soft matter. *Liquid Crystals*, 42(5-6), pp.593-622.
- [18] Glaser, M.A. and Clark, N.A., 2002. Fluctuations and clinicity in tilted smectic liquid crystals. *Physical Review E*, 66(2), p.021711.